

LETTERS

Spontaneous symmetry breaking in a quenched ferromagnetic spinor Bose–Einstein condensate

L. E. Sadler¹, J. M. Higbie¹, S. R. Leslie¹, M. Vengalattore¹ & D. M. Stamper-Kurn¹

A central goal in condensed matter and modern atomic physics is the exploration of quantum phases of matter—in particular, how the universal characteristics of zero-temperature quantum phase transitions differ from those established for thermal phase transitions at non-zero temperature. Compared to conventional condensed matter systems, atomic gases provide a unique opportunity to explore quantum dynamics far from equilibrium. For example, gaseous spinor Bose–Einstein condensates^{1–3} (whose atoms have non-zero internal angular momentum) are quantum fluids that simultaneously realize superfluidity and magnetism, both of which are associated with symmetry breaking. Here we explore spontaneous symmetry breaking in ⁸⁷Rb spinor condensates, rapidly quenched across a quantum phase transition to a ferromagnetic state. We observe the formation of spin textures, ferromagnetic domains and domain walls, and demonstrate phase-sensitive *in situ* detection of spin vortices. The latter are topological defects resulting from the symmetry breaking, containing non-zero spin current but no net mass current⁴.

Spinor atomic gases^{1–3} are those comprised of atoms with non-zero internal angular momentum—the sum of electronic and nuclear angular momenta, denoted by quantum number F —and in which all orientations of the atomic spin may be realized. A spinor gas Bose–Einstein condensate (BEC) is described by a vector order parameter and therefore exhibits spontaneous magnetic ordering. Nevertheless, freedom remains for the type of ordering that can occur. For ⁸⁷Rb $F = 1$ spinor gases^{5,6}, the spin-dependent energy per particle in the condensate is the sum of two terms, $c_2 n \langle \hat{\mathbf{F}} \rangle^2 + q \langle \hat{F}_z^2 \rangle$, where $\hat{\mathbf{F}}$ denotes the dimensionless spin vector operator. The first term describes spin-dependent interatomic interactions, with n being the number density and $c_2 = (4\pi\hbar^2/3m)(a_s - a_0)$ depending on the atomic mass m and the s -wave scattering lengths a_f for collisions between pairs of particles with total spin f (refs 2 and 3). Given $c_2 < 0$ for our system^{5–7}, the interaction term alone favours a ferromagnetic phase with broken rotational symmetry. The second term describes a quadratic Zeeman shift in our experiment, with $q = (h \times 70 \text{ Hz G}^{-2}) B^2$ at a magnetic field of magnitude B (the linear Zeeman shift may be neglected owing to spin conservation). This term favours instead a phase with no net magnetization, that is, a condensate in the $|m_z = 0\rangle$ magnetic sublevel, with unbroken $O(2)$ rotational symmetry in the transverse spin plane. These two phases have distinct symmetries, and are therefore divided by a quantum phase transition at $q = 2|c_2|n$.

Here we describe the observation of spontaneous symmetry breaking in a ⁸⁷Rb spinor BEC that is rapidly quenched across this quantum phase transition. Nearly pure spinor BECs were prepared in the unmagnetized $|m_z = 0\rangle$ phase at a high quadratic Zeeman shift ($q \gg 2|c_2|n$). By rapidly reducing the magnitude of the applied magnetic field, we quenched the gas to conditions that favour the ferromagnetic phase ($q \ll 2|c_2|n$). At variable times T_{hold} after the

quench, high-resolution maps of the magnetization vector density were obtained using magnetization-sensitive phase-contrast imaging⁸. After the quench, transverse ferromagnetic domains of variable size formed spontaneously throughout the condensate, divided by narrow unmagnetized domain walls. Concurrent with the formation of these domains, we also observed topological defects that we characterize as singly charged spin vortices with circulating spin currents and unmagnetized filled cores.

Spinor BECs in the $|F = 1, m_z = 0\rangle$ hyperfine state were confined in an optical dipole trap characterized by oscillation frequencies $(\omega_x, \omega_y, \omega_z) = 2\pi(56, 350, 4.3) \text{ s}^{-1}$. The condensates, typically containing $2.1(1) \times 10^6$ atoms, were formed at a magnetic field of 2 G and characterized by a peak density $n_0 = 2.8 \times 10^{14} \text{ cm}^{-3}$ and Thomas–Fermi radii $(r_x, r_y, r_z) = (12.8, 2.0, 167) \mu\text{m}$ (see Methods). Variations in the internal-state wavefunction were constrained in these anisotropic condensates to just two spatial dimensions (\hat{x} and \hat{z}) because the spin healing length, $\xi_s = \sqrt{\hbar^2/2m|c_2|n_0} = 2.4 \mu\text{m}$, was larger than the cloud size r_y in the \hat{y} direction. Thus, imaging the condensate in the \hat{x} – \hat{z} plane produced complete maps of the magnetization density.

After the condensate was formed, the magnetic field was oriented in the \hat{z} direction, ramped linearly over 5 ms to a magnitude of 50 mG, and held at this setting for a variable time T_{hold} before we imaged the gas. At this field, the quadratic Zeeman energy $q = h \times 0.2 \text{ Hz}$ is negligible compared to twice the spin-dependent interaction energy of $2|c_2|\langle n \rangle_y = h \times 16 \text{ Hz}$, where $\langle n \rangle_y$ is the density averaged in the \hat{y} direction.

The condensate magnetization was measured *in situ* using phase-contrast imaging, which yields a magnetization-sensitive signal given approximately as ζF_y , where ζ is proportional to the gas column density and $F_y = \langle \hat{F}_y \rangle$ is one component of the (dimensionless) magnetization of the gas (see Methods). We determined all three components of the vector magnetization density with repeated imaging of the same atomic sample. Transverse magnetization was detected by imaging its Larmor precession about a \hat{z} -oriented guide field⁸. The complex transverse magnetization $F_t = F_x + iF_y$ was then determined as $A(\boldsymbol{\rho}) \exp(i\phi(\boldsymbol{\rho})) = i\zeta(\boldsymbol{\rho})F_t(\boldsymbol{\rho})$ from the amplitude $A(\boldsymbol{\rho})$ and phase of $\phi(\boldsymbol{\rho})$ of Larmor precession at each pixel position $\boldsymbol{\rho}$. Longitudinal magnetization was then measured from images in which the magnetic field was adiabatically reoriented in the $\pm\hat{y}$ directions.

As shown in Fig. 1, at short times after the quench ($T_{\text{hold}} < 50 \text{ ms}$), images probing the transverse magnetization show no significant variation across the cloud or between frames (similarly for the longitudinal magnetization images), indicating the presence of BECs remaining in the unmagnetized phase. Any magnetization during this stage was either too low in magnitude or varied over too short a length scale to be discerned by our imaging. At later times, a non-zero transverse magnetization signal spontaneously developed,

¹Department of Physics, University of California, Berkeley, California 94720, USA.

yielding a Larmor precession signal that varied both in amplitude and in phase across the condensate. This observation indicates heterogeneous, spontaneous symmetry breaking in the gas, specifically the breaking of $O(2)$ rotational symmetry in the transverse plane in a direction given by the phase of Larmor precession.

In Fig. 2, the derived transverse magnetization for samples at variable times T_{hold} are presented, rendered in colour to portray both the magnetization orientation (as hue) and amplitude (as brightness). These spatial maps show ferromagnetic domains of variable size and orientation arising spontaneously after the quench. The landscape of domains includes small regions of homogeneous magnetization, with unmagnetized domain walls separating regions of nearly opposite orientation, and also larger ferromagnetic spin textures free of domain walls in which the magnetization orientation varies smoothly over tens of micrometres.

Ferromagnetic domains from a quenched unmagnetized ($|m_z = 0\rangle$) gas arise through a dynamical instability in a spinor BEC^{9–12}. This instability, which is a consequence of coherent collisional mixing between magnetic sublevels^{5,6,13,14}, may also be regarded as the phase separation of a two-component condensate^{15,16}. For this, we recall that the $|m_z = 0\rangle$ state represents a coherent superposition of the $|m_\phi = \pm 1\rangle$ eigenstates of any transverse spin operator, $\hat{F}_\phi = \hat{F}_x \cos \phi + \hat{F}_y \sin \phi$, and that, because $c_2 < 0$, the ± 1 eigenstates of any spin component are immiscible¹⁷. Ferromagnetism thus arises by the spinodal decomposition of a binary gaseous mixture into neighbouring regions of oppositely oriented transverse magnetization. This phase separation is dominated by a fast-growing instability with an exponential timescale of $\tau_{\text{fm}} = \hbar / \sqrt{2|c_2|n}$. The wavevector of the dominant instability $k_{\text{fm}} = \sqrt{2m|c_2|n}/\hbar$ defines the typical size $l = \pi k_{\text{fm}}^{-1}$ of single-component domains in the phase-separated fluid, and also the width $b \approx k_{\text{fm}}^{-1}$ of domain walls in which the two components still overlap^{18,19}.

We emphasize that domain formation is neither the cause nor the mechanism for spontaneous symmetry breaking. In the context of mean-field theory, the above mentioned dynamical instability describes the amplification of an initial seed of non-zero transverse

magnetization of a particular spin orientation (denoted above as ϕ) once the rotational symmetry of the initial unmagnetized gas is already broken. The source of such a symmetry-broken seed is either thermal or quantum magnetization fluctuations in the gas before the quench. In this work, the forced depletion of atoms not in the $|m_z = 0\rangle$ state and the energy gap for magnetization fluctuations in the unmagnetized (high- q) phase suggest that ferromagnetism formed purely by the amplification of quantum fluctuations, that is, shot noise, a suggestion that warrants experimental justification.

To compare our data to the model of dynamical instabilities described above, we considered the density-weighted transverse magnetization correlation function:

$$G_t(\delta\rho) = \text{Re} \left[\frac{\sum_{\rho} (\zeta(\rho) F_t(\rho))^* (\zeta(\rho + \delta\rho) F_t(\rho + \delta\rho))}{\sum_{\rho} \zeta(\rho) \zeta(\rho + \delta\rho)} \right]$$

At zero range, $G_t(0)$ measures the degree to which the condensate has evolved toward the ferromagnetic state. As shown in Fig. 3a, $G_t(0)$ rises after the quench from a near-zero value characteristic of the unmagnetized state to a nearly constant value of $G_t(0) \approx 0.5$. This saturation value measures the area occupied by domain walls. Fitting $G_t(0)$ at early times ($T_{\text{hold}} < 90$ ms) to a rising exponential yields a time constant of $\tau = 15(4)$ ms, in agreement with the predicted $\tau_{\text{fm}} = \hbar / \sqrt{2|c_2|n} = 13.7(3)$ ms. Over the same period of evolution, no significant longitudinal magnetization was observed, confirming the presence of purely transverse ferromagnetic domains.

Spatial correlations in the transverse magnetization (Fig. 3b) are

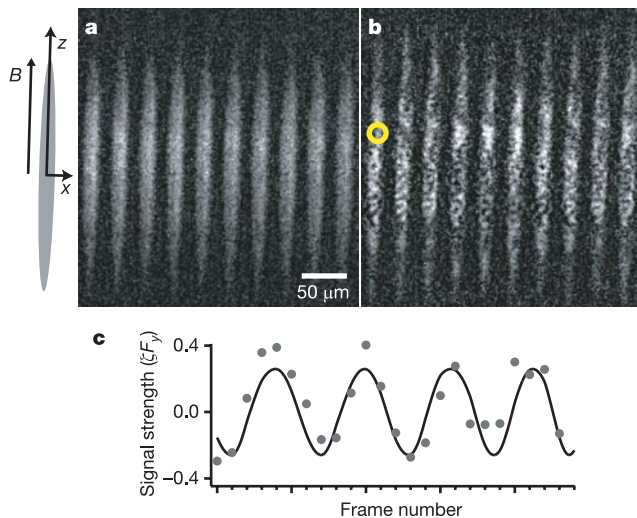


Figure 1 | Direct imaging of inhomogeneous spontaneous magnetization of a spinor BEC. Transverse imaging sequences (first 10 of 24 frames) are shown for a single condensate probed at $T_{\text{hold}} = 36$ ms (a) and for a different condensate at $T_{\text{hold}} = 216$ ms (b). Shortly after the quench, the system remains unmagnetized, showing neither short-range spatial nor temporal variation (that is, between frames). In contrast, condensates at longer times are spatially inhomogeneous and display spontaneous Larmor precession. The precession signal from one pixel position (at centre of yellow circle in b) is presented in c with data (circles) and fitted precession (line) both shown. Orientations of axes and magnetic field are shown on the left.

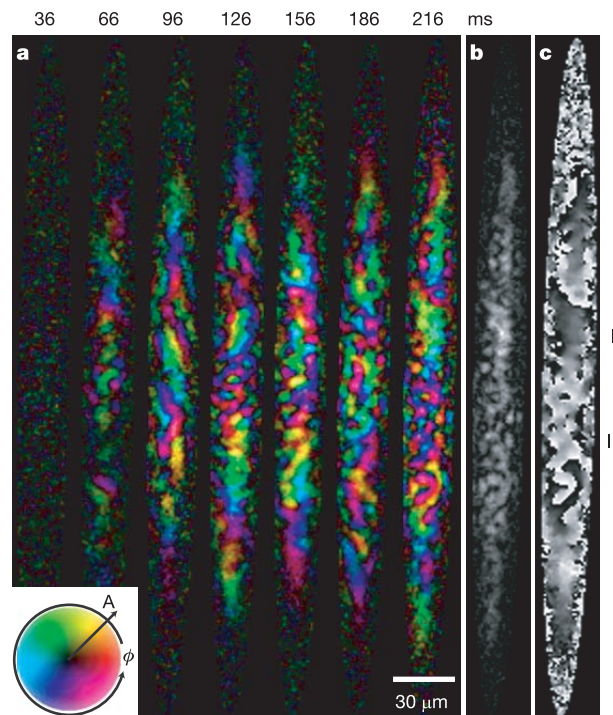


Figure 2 | In situ images of ferromagnetic domains and domain walls. a, The transverse magnetization density, measured for condensates at variable times T_{hold} (given on top), is shown with the magnetization orientation ($\phi = \arg(F_t)$) indicated by hue, and magnitude ($A = \zeta|F_t|$) by brightness. The maximum brightness, shown by the colour wheel on the left, corresponds to full magnetization of the condensate centre. For the data at $T_{\text{hold}} = 216$ ms, the magnetization density (b) and orientation (c) are shown separately. The spin texture at position I is characterized by an extended region (along \hat{z}) of non-zero magnetization magnitude, and a slowly varying magnetization orientation. Smaller magnetic domains at position II are divided by domain walls with zero magnetization. The greyscale in c covers the range 0 to 2π . Regions outside the condensate are coloured in black.

typified by a central region of positive correlations (near $\delta\rho = 0$) and then several equally sized regions of alternating negative and positive correlations displaced from one another in the narrow \hat{x} dimension of the condensate. We estimate a typical size for single-component domains as $\approx 10\ \mu\text{m}$, twice the displacement at which the transverse spin–spin correlation changes sign, in good agreement with the predicted $\pi k_{\text{fm}}^{-1} = 8.3(2)\ \mu\text{m}$. The presence of negative correlation regions supports the model of spin-conserving phase separation discussed above. The preferential phase separation in the narrow \hat{x} direction rather than along \hat{z} , as indicated by $G_t(\delta\rho)$, may arise because the momentum distribution of the unmagnetized condensate in that direction is broader owing to the finite condensate size. Thus, upon quenching the system, a greater population of atoms is available to seed the faster-growing, shorter-wavelength instabilities with wavevector in the \hat{x} direction. The presence of several alternations of positive and negative correlations further suggests that the phase separation occurs through a small number of discrete, unstable magnetization modes.

The spontaneous symmetry breaking observed in this work is one of many examples of symmetry breaking that occur in nature. For example, symmetry breaking is presumed to have occurred at thermal phase transitions in the early Universe, giving rise to the specific elementary particles and interactions now observed. An important aspect of rapid spontaneous symmetry breaking, whether in the laboratory or of a cosmological nature, is the creation of topological defects^{20–22}. The types of topological defects that may be formed depend on the group structure of the ground-state manifold reached at the transition.

Analogues of cosmological topological defect formation have been studied using liquid crystals²³ and superfluid helium^{24–26}. In

comparison with these previous experiments, the present investigation focuses on a simpler physical system, in which the time for thermal equilibration and domain formation is much longer than that needed to bring the system across the symmetry-breaking transition. Furthermore, the present work focuses on a quantum rather than a thermal phase transition²².

In our two-dimensional system, spin vortices are topological point defects about which the orientation of magnetization has a $2\pi l$ winding with l being a non-zero integer. Spin-vortex defects were observed with high confidence in about one-third of all images containing significant ferromagnetism ($T_{\text{hold}} > 90\ \text{ms}$), with some images indicating as many as four vortices (see Methods). Data revealing one such spin vortex are shown in Fig. 4. For this vortex, the central region of near-zero Larmor precession amplitude has a diameter of about $3\ \mu\text{m}$, comparable to the spin healing length $\xi_s = 2.4\ \mu\text{m}$ defined earlier. All observed vortices were singly quantized, with no apparent preferred direction of circulation.

Many types of vortices that can occur in a gas with a multi-component order parameter can be distinguished by the composition of their cores²⁷. On the basis of our measurements of the transverse and longitudinal magnetization at the vortex core, the spin vortices seen in our experiment appear to have unmagnetized filled cores. This observation supports their characterization as ‘polar-core’ spin vortices (denoted as $(\pm 1, 0, \mp 1)$ vortices in ref. 27), for which the superfluid order parameter is a superposition of atoms in the $|m_z = 1\rangle$ state rotating with one quantum of circulation, atoms in the $|m_z = -1\rangle$ state rotating with one quantum of circulation in the opposite sense, and non-rotating atoms in the unmagnetized $|m_z = 0\rangle$ state, which also fill the vortex core. Such a vortex is thus characterized by zero net mass circulation and a spin current with one quantum of circulation. The origin for such spin currents is presumably the spinodal decomposition by which ferromagnetism emerges from the unmagnetized cloud. The generation of such vortices under conditions of our experiment was predicted in ref. 4. The alternate identification of these vortices as merons²⁸ is ruled out by the absence of longitudinal magnetization at the vortex core.

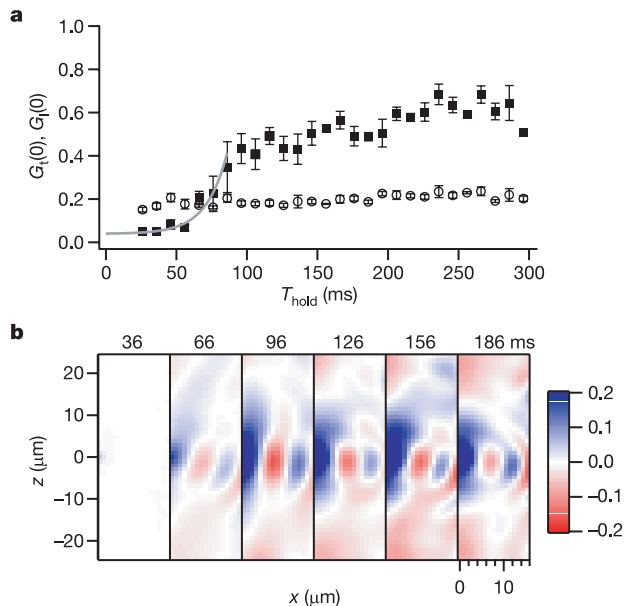


Figure 3 | Temporal and spatial evolution of ferromagnetism in a quenched spinor BEC. **a**, The mean local squared transverse ($G_t(0)$, squares) and longitudinal ($G_1(0)$, circles) magnetization, averaged over several experimental repetitions (error bars indicate shot-to-shot root-mean-square fluctuations), is shown. $G_t(0)$ rises exponentially with time constant $\tau = 15(4)$ ms as determined by a fit to data for $T_{\text{hold}} < 90$ ms (grey line), and saturates at $G_t(0) \approx 0.5$ at later times. No significant longitudinal magnetization is observed. The minimum values for $G_t(0)$ and $G_1(0)$, evident in the data for earliest T_{hold} , reflect residual noise due to processing either 24 or 2 frames, respectively, to obtain the magnetization density. **b**, Spatial correlation in the transverse magnetization ($G_t(x, z)$), at variable T_{hold} shows alternating regions of positive and negative correlations in the narrow \hat{x} direction. At each T_{hold} , $G_t(x, z)$ was determined for ten experimental repetitions and then averaged.

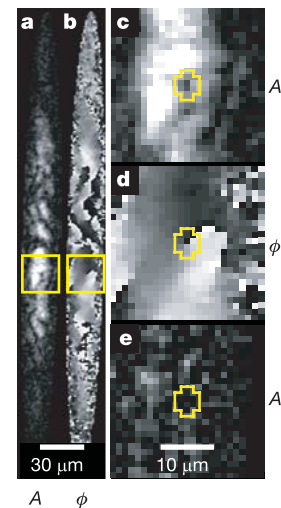


Figure 4 | In situ detection of a polar-core spin vortex. Spatial maps of the transverse magnetization magnitude ($A = \zeta|F_t|$) (**a**) and orientation ($\phi = \arg(F_t)$) (**b**) are shown for a sample imaged at $T_{\text{hold}} = 156$ ms. Data from a portion of the condensate, indicated by boxes, are magnified, showing the transverse magnetization magnitude (**c**) and orientation (**d**) and also the magnitude of the longitudinal magnetization ($A_l = \zeta|F_z|$) (**e**). The phase along a closed path (indicated in yellow) surrounding a region of near-zero transverse magnetization shows a net winding of 2π , revealing the presence of a spin-vortex defect. The core (within the closed path) shows no significant longitudinal magnetization, allowing the identification of the defect as a polar-core spin vortex. The greyscale for images **a**, **c** and **e** is the same.

In contrast with their topological nature in some other magnetic systems, domain walls in a $F = 1$ ferromagnet are not topologically stable; rather, they may decay by the formation of spin vortex–antivortex pairs. However, we observe domain walls that form at the onset of visible ferromagnetism in the gas and persist for all times thereafter. In future experiments, our non-destructive imaging method may be adapted to allow the behaviour of a single quenched condensate to be recorded, allowing a closer examination of the dynamical evolution of domain walls. Improved magnetization imaging may allow studies of hourspin vortices are produced^{20,21} and of their subsequent evolution. Further time-resolved experiments in which one varies the rate at which the system is swept into the ferromagnetic state may also uncover universal temporal dynamics that typify this and other quantum phase transitions.

METHODS

Experimental sequence. Optically trapped BECs were obtained by loading around 10^8 atoms in the $|F = 1, m_z = -1\rangle$ state with temperature of $2.5 \mu\text{K}$ into an optical dipole trap. The optical trap was formed by a single focused laser beam with a wavelength of 825 nm, which was linearly polarized to ensure that all components experience the same trap potential. A small shift quadratic in m_F from the optical beam was negligible.

Using radio-frequency rapid adiabatic passage followed by application of a transient magnetic field gradient of 4 G cm^{-1} , all atoms in the optical trap were placed in the $|m_z = 0\rangle$ magnetic sublevel. While the magnetic field was held at a magnitude of 2 G, the trap depth was decreased over 400 ms to $k_B \times 350 \text{ nK}$ and the temperature of the gas to $\sim 40 \text{ nK}$, well below the Bose–Einstein condensation temperature. This yielded nearly pure condensates of $2.1(1) \times 10^6$ atoms.

At the low-field setting following the quench, magnetic field gradients along the \hat{x} and \hat{z} directions were nulled to less than 0.2 mG cm^{-1} . A Stern–Gerlach analysis of populations in each of the magnetic sublevels was applied to establish that the field ramp was sufficiently slow so as not to alter the spin state of the condensate. Such an analysis bounded the populations in each of the $|m_z = \pm 1\rangle$ spin states to be less than 0.3% of the total population, both before and right after the field ramp. At later times T_{hold} after the quench, such measurements showed significant mixing of populations coincident with the onset of spontaneous Larmor precession^{5,6}.

Magnetization imaging. The probe light for magnetization-sensitive phase-contrast imaging was circularly polarized and detuned by $\delta = -200 \text{ MHz}$ from the $5S_{1/2}(F = 1) \rightarrow 5P_{1/2}(F' = 2)$ transition. At this setting, the phase-contrast signal is given approximately as $\zeta(\frac{\delta}{5} + \langle \hat{F}_x \rangle + \frac{1}{5} \langle \hat{F}_y^2 \rangle)$ where $\zeta = (5/48)\tilde{n}\sigma\gamma/\delta$, \tilde{n} is the column density of the gas, $\sigma = 3\lambda^2/2\pi$ is the resonant cross-section, $\lambda = 795 \text{ nm}$ is the wavelength of the probe light, and γ is the natural linewidth. We ignore the small $\langle \hat{F}_y^2 \rangle$ signal in this work. Probe pulses were $1 \mu\text{s}$ in duration, much shorter than the $\sim 35 \text{ kHz}$ Larmor precession frequency at a 50 mG field. The imaging system was diffraction-limited, with a resolution defined by the modulation transfer function dropping to half for features with pitch $6 \mu\text{m}$ in the object plane. Sufficient magnification was used so that the finite pixel-size of our camera caused no degradation of the image.

The image sequence began with 24 images taken of the same atomic sample at a strobe frequency of 10 kHz while the magnetic field remained oriented along the \hat{z} direction. These images were used to measure the orientation and magnitude of the transverse magnetization. The normalization constant $\zeta(\rho)$ was obtained by averaging the signal over all image frames and fitting with a Thomas–Fermi distribution for the density of the condensate. Following this sequence, two additional image frames were obtained within 5 ms in which the magnetic field was adiabatically reoriented in the \hat{y} and $-\hat{y}$ directions. The longitudinal magnetization was determined from the difference between these last frames.

Image analysis. The identification of spin vortices in the magnetization images relied on the identification of a core of ‘dark’ pixels, consistent with zero Larmor precession amplitude, which were surrounded by ‘bright’ pixels with a finite amplitude and well-defined phase of Larmor precession. We identified vortices based on two criteria: (1) that there be an island of dark pixels, a candidate for the vortex core, which is surrounded entirely by bright pixels and that is at least two bright pixels away from nearby dark pixels, and (2) that the transverse magnetization traced along a closed loop through bright pixels surrounding

the core have a non-zero net winding. The distinction between bright and dark pixels (at about one-quarter of the maximum Larmor precession amplitude) was chosen to eliminate false-positive vortex detections in simulated data taking into account the measured noise (optical shot-noise limited) and resolution of our imaging system, and using estimates for the width of contiguous domain walls.

Received 23 March; accepted 20 July 2006.

1. Stenger, J. *et al.* Spin domains in ground state spinor Bose–Einstein condensates. *Nature* **396**, 345–348 (1998).
2. Ho, T.-L. Spinor Bose condensates in optical traps. *Phys. Rev. Lett.* **81**, 742–745 (1998).
3. Ohmi, T. & Machida, K. Bose–Einstein condensation with internal degrees of freedom in alkali atom gases. *J. Phys. Soc. Jpn* **67**, 1822–1825 (1998).
4. Saito, H., Kawaguchi, Y. & Ueda, M. Breaking of chiral symmetry and spontaneous rotation in a spinor Bose–Einstein condensate. *Phys. Rev. Lett.* **96**, 065302 (2006).
5. Chang, M.-S. *et al.* Observation of spinor dynamics in optically trapped Rb Bose–Einstein condensates. *Phys. Rev. Lett.* **92**, 140403 (2004).
6. Schmaljohann, H. *et al.* Dynamics of $F = 2$ spinor Bose–Einstein condensates. *Phys. Rev. Lett.* **92**, 040402 (2004).
7. Klausen, N. N., Bohn, J. L. & Greene, C. H. Nature of spinor Bose–Einstein condensates in rubidium. *Phys. Rev. A* **64**, 053602 (2001).
8. Higbie, J. M. *et al.* Direct, non-destructive imaging of magnetization in a spin-1 Bose gas. *Phys. Rev. Lett.* **95**, 050401 (2005).
9. Pu, H. *et al.* Spin-mixing dynamics of a spinor Bose–Einstein condensate. *Phys. Rev. A* **60**, 1463–1470 (1999).
10. Robins, N. P., Zhang, W., Ostrovskaya, E. A. & Kivshar, Y. S. Modulational instability of spinor condensates. *Phys. Rev. A* **64**, 021601(R) (2001).
11. Saito, H. & Ueda, M. Spontaneous magnetization and structure formation in a spin-1 ferromagnetic Bose–Einstein condensate. *Phys. Rev. A* **72**, 023610 (2005).
12. Zhang, W. *et al.* Dynamical instability and domain formation in a spin-1 Bose–Einstein condensate. *Phys. Rev. Lett.* **95**, 180403 (2005).
13. Widera, A. *et al.* Coherent collisional spin dynamics in optical lattices. *Phys. Rev. Lett.* **95**, 190405 (2005).
14. Chang, M.-S. *et al.* Coherent spinor dynamics in a spin-1 Bose condensate. *Nature Phys.* **1**, 111–116 (2005).
15. Hall, D. S. *et al.* The dynamics of component separation in a binary mixture of Bose–Einstein condensates. *Phys. Rev. Lett.* **81**, 1539–1542 (1998).
16. Miesner, H.-J. *et al.* Observation of metastable states in spinor Bose–Einstein condensates. *Phys. Rev. Lett.* **82**, 2228–2231 (1999).
17. Stamper-Kurn, D. M. & Ketterle, W. in *Coherent Matter Waves* (eds Kaiser, R., Westbrook, C. & David, F.) 137–218 (Springer, New York, 2001).
18. Goldstein, E. V. & Meystre, P. Quasiparticle instabilities in multicomponent atomic condensates. *Phys. Rev. A* **55**, 2935–2940 (1997).
19. Timmermans, E. Phase separation of Bose–Einstein condensates. *Phys. Rev. Lett.* **81**, 5718–5721 (1997).
20. Kibble, T. W. B. Topology of cosmic domains and strings. *J. Phys. A* **9**, 1387–1398 (1976).
21. Zurek, W. H. Cosmological experiments in superfluid helium? *Nature* **317**, 505–508 (1985).
22. Zurek, W. H., Dornier, U. & Zoller, P. Dynamics of a quantum phase transition. *Phys. Rev. Lett.* **95**, 105701 (2005).
23. Chuang, I., Durrer, R., Turok, N. & Yurke, B. Cosmology in the laboratory: defect dynamics in liquid crystals. *Science* **251**, 1336–1342 (1991).
24. Hendry, P. C. *et al.* Generation of defects in superfluid ^4He as an analogue of the formation of cosmic strings. *Nature* **368**, 315–317 (1994).
25. Ruutu, V. M. H. *et al.* Vortex formation in neutron-irradiated superfluid He-3 as an analogue of cosmological defect formation. *Nature* **382**, 334–336 (1996).
26. Bauerle, C. *et al.* Laboratory simulation of cosmic string formation in the early Universe using superfluid He-3. *Nature* **382**, 332–334 (1996).
27. Isoshima, T., Machida, K. & Ohmi, T. Quantum vortex in a spinor Bose–Einstein condensate. *J. Phys. Soc. Jpn* **70**, 1604–1610 (2001).
28. Mermin, N. D. & Ho, T.-L. Circulation and angular momentum in the A phase of superfluid helium-3. *Phys. Rev. Lett.* **36**, 594–597 (1976).

Acknowledgements We thank E. Mueller, J. Moore, and A. Vishwanath for comments, J. Guzman for experimental assistance, and the NSF and the David and Lucile Packard Foundation for financial support. S.R.L. acknowledges support from the NSERC.

Author Information Reprints and permissions information is available at www.nature.com/reprints. The authors declare no competing financial interests. Correspondence and requests for materials should be addressed to D.M.S.-K. (dmsk@berkeley.edu).